

Cite this: *RSC Adv.*, 2015, 5, 8571

Magnetically retrievable lepidocrocite supported copper oxide nanocatalyst (Fe–CuO) for *N*-arylation of imidazole†

R. Sivakami,^a S. Ganesh Babu,^c S. Dhanuskodi^{*a} and R. Karvembu^{*b}

A simple and efficient lepidocrocite-supported copper oxide catalyst (Fe–CuO) has been successfully prepared by a simple precipitation method in aqueous medium from readily available inexpensive starting materials and was used as a heterogeneous nanocatalyst for the *N*-arylation of imidazole with various aryl halides. The morphology, crystal structure, magnetic property, chemical state and surface area of the catalyst were studied. The *N*-arylation reaction was chosen to demonstrate the catalytic efficiency of the as-prepared Fe–CuO. Importantly, the catalyst can be easily recovered by magnetic attraction and its catalytic activity remains unaltered even after 6 consecutive cycles. Hence, Fe–CuO is an environmentally friendly, easily applicable and cost effective catalyst.

Received 27th October 2014
Accepted 11th December 2014

DOI: 10.1039/c4ra13256d

www.rsc.org/advances

Introduction

Transition-metals-catalyzed cross-coupling reactions represent one of the robust methods for the formation of carbon–carbon and carbon–heteroatom bonds.¹ Particularly, the synthesis of *N*-arylimidazole attracted significant interest because of the frequent occurrence of these structural units in biologically active inhibitors.² *N*-Arylimidazole is not only important in biological systems but is also a common moiety in pharmaceutical research. A significant number of *N*-arylimidazole derivatives have been reported to have biomedical applications; serve as cyclic AMP phosphodiesterase inhibitors,³ AMPA receptor antagonists,⁴ cardio tonic agents,⁵ thromboxane synthases inhibitors⁶ and topical antiglaucoma agents.⁷ Therefore, their preparation has attracted much attention. In recent years, the homogeneous Pd-catalyzed *N*-arylation of imidazole has made remarkable achievements, and is performed under relatively mild reaction conditions.⁸ In spite of having wide scope and excellent compatibility with many functional groups, these protocols often suffer from the disadvantages resulting from (i) the high cost of the Pd precursors, (ii) the need for ancillary ligands, (iii) the toxicity of Pd salts and (iv) the extended reaction times.

In addition, higher stoichiometric amounts of Pd catalyst are often required. To circumvent these issues, newer and milder

homogeneous transition metal catalysts have been developed. The major drawback of homogeneous catalysts is difficulty in separation from the product and/or reaction medium and thus product purification, recovery and regeneration of catalyst are very difficult.⁹ Nowadays, heterogeneous catalysts particularly metal nanoparticles (MNPs) including CuO with high surface area are getting so much attention from both economic and industrial point of view because they possess very good activity and are highly recyclable.^{10,11} Despite of their advantages, drawbacks remain in these catalysts too, as the metal nanoparticles effortlessly agglomerate during the reaction and are less stable under severe reaction conditions, which lead to low catalytic activity as well as poor reusability of the catalysts.¹² To prevent the agglomeration of metal nanoparticles and the over-stoichiometric use of Cu reagents, several inorganic materials such as alumina and silica have been used as a support for metal nano particles, but again they have limited stability under both acidic and basic conditions.¹³ Therefore, developing an efficient and recyclable catalyst for the *N*-arylation of heterocycles with the use of lower amount of Cu remains a challenging one. Magnetically active nano particles have recently emerged as viable alternatives to conventional catalyst supports.^{14,15} On the other hand, magnetic nanocomposites serve both as the support and stabilizer for the nanoparticles, thus providing a better chance to prevent aggregation. Furthermore, magnetic separation is an alternative to filtration or centrifugation as it prevents loss of catalyst and increases the reusability.¹⁶ Iron oxides, such as magnetite, hematite and some other iron oxides have been well investigated as catalysts or supports in various important organic transformations.^{17–20} For instance, copper on iron oxide was used for the synthesis of propargylamines²¹ and Pd-magnetite was exploited in carbonylative Sonogashira coupling reaction.²² In recent years, copper based catalysts/

^aSchool of Physics, Bharathidasan University, Tiruchirappalli-620 024, India. E-mail: dhanus2k3@yahoo.com

^bDepartment of Chemistry, National Institute of Technology, Tiruchirappalli-620 015, India. E-mail: kar@nitt.edu

^cSRM Research Institute, SRM University, Kattankulathur 603203, Chennai, India

† Electronic supplementary information (ESI) available. See DOI: 10.1039/c4ra13256d

nanocatalysts are widely employed in various organic processes and catalytic reactions^{23–26} including energy conversion.²⁷ However less attention has been focused on the catalytic applications of Fe–CuO. We believe that Fe–CuO magnetic nanocatalyst could overcome the drawbacks exist in the *N*-arylation of heterocycles. Herein we describe an inexpensive, stable, magnetically separable and recyclable Fe–CuO nanocatalyst for *N*-arylation reaction of imidazole with various aryl halides under ligand-free condition. This system provides a simplified procedure for the isolation of the catalyst.

Results and discussion

The lepidocrocite and Fe–CuO were prepared following the literature.²⁸ After drying the resulting material, the initial investigation was focused on the characterization of the solid material. Based on the inductively coupled plasma optical emission spectroscopic (ICP-OES) analysis, the amount of Cu and Fe were found to be 0.431 and 0.602 mol g^{−1} respectively in Fe–CuO.

The crystallinity of the γ -FeOOH and Fe–CuO was examined by powder X-ray diffraction. The XRD peaks correspond to single orthorhombic phase. The crystallite size of the γ -FeOOH and Fe–CuO was found to be 47 and 41 nm (calculated using Scherrer's equation), respectively.

FT-IR confirms the Cu substitution in the γ -FeOOH nanoparticles^{29–32} (see ESI – S1†). SEM images of γ -FeOOH and Fe–CuO reveal the compact arrangement of nanoparticles with spherical shape (see ESI – S2†). Elemental composition obtained from the EDAX analysis shows that the weight percentage of Cu is around 4.9 in Fe–CuO. TEM images revealed that the particle size of as prepared (7 nm) and calcined at 500 °C for 3 h (32 nm) Fe–CuO nanocomposites (Fig. 3). Images show the agglomeration of the nanoparticles, which may be attributed to the interactions among the magnetic particles.³³

XPS spectra of Fe–CuO are displayed in Fig. 4(i–iv). As seen in Fig. 4(i), the wide XPS spectrum reveals the presence of Fe, Cu and O elements. The curve fitting was performed on Fe, Cu and O 1s spectra of Fe–CuO using a Gaussian–Lorentzian peak

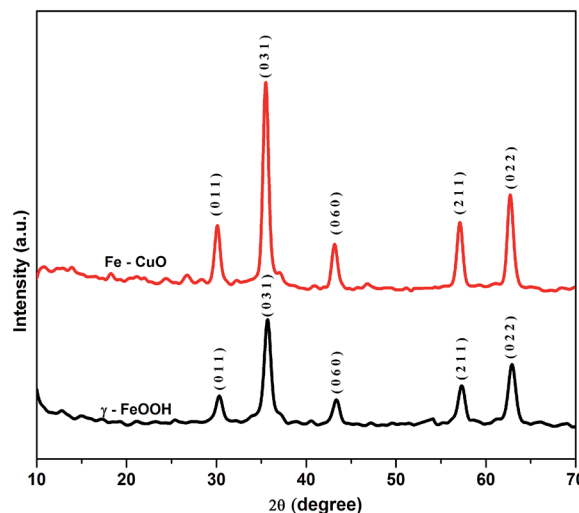


Fig. 2 XRD pattern of γ -FeOOH and Fe–CuO.

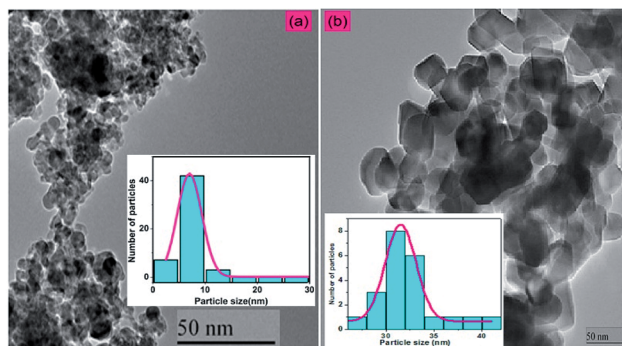


Fig. 3 TEM images of Fe–CuO nanocatalyst (a) as prepared and (b) calcined at 500 °C for 3 h [inset is the particle size distribution].

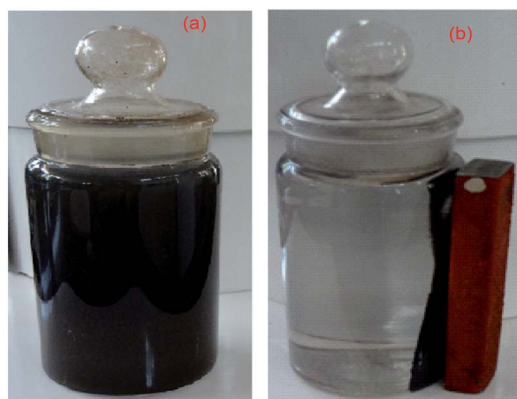


Fig. 1 Photograph of the (a) catalyst dispersed in the reaction mixture and (b) magnetic separation of the catalyst from the reaction medium.

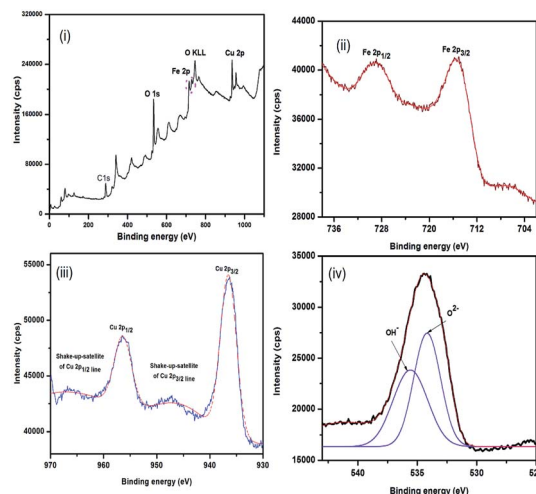


Fig. 4 XPS spectra of Fe–CuO nanocatalyst (i) XPS survey spectrum, (ii) main peaks of Fe 2p (iii) main peaks of Cu 2p and (iv) O 1s spectra.

shape. Fig. 4(ii) shows the Fe 2p core level spectrum. The peaks located at 713.39 eV for Fe 2p_{3/2} and 726.02 eV for Fe 2p_{1/2} are ascribed to the presence of Fe³⁺ ions in FeOOH. These values are in good agreement with the reported data.³⁴

In Fig. 4(iii), the peaks at the binding energies of 956.2 and 936.3 eV accompanying with their shakeup satellites, correspond to Cu 2p_{1/2} and Cu 2p_{3/2}, which proved the presence of Cu²⁺ ions³⁵ and thereby confirmed the formation of CuO. In fact, the shake-up satellite feature is peculiar to CuO that relates to d⁹ configuration of ground state of the Cu. Fitting of the oxygen region produced two O 1s peaks. In Fig. 4(iv), the peak at 530.80 eV corresponds to O²⁻ in the lattice. Similarly the peak at 532.54 eV is due to surface hydroxyl groups or chemisorbed water molecules.³⁶ The peak at 289 eV is attributed to C 1s spectra. This proves that there has been a strong interaction between lepidocrocite and CuO nanoparticles.

The Raman spectrum (see ESI – S3†) confirms the presence of Fe and Cu nanoparticles in the material. The band positions of the Fe and Cu phases are in excellent match with the literature values.^{37,38} Thermal stability of the catalyst was found to be stable up to 1000 °C by TG/DTA^{39–41} (see ESI – S3†).

The ferromagnetic behaviour was confirmed using magnetization curves of γ-FeOOH and Fe–CuO at room temperature. The observed saturation magnetization (*M_s*) and coercivity (*H_c*) values have been summarized in table [inset Fig. S5] (see ESI – S5†). The increase of saturation magnetization for CuO loaded sample is due to the higher surface electron spins. The CuO added sample showed reduction in coercive field. This may be due to the effect of CuO into the domains of γ-FeOOH.⁴²

After the successful preparation and characterization of Fe–CuO, its catalytic activity was examined for *N*-arylation of imidazole with 4-bromobenzonitrile. Initially, the reaction conditions such as base, solvent, reaction time and reaction temperature were optimized. The results showed that 120 °C was required for the coupling reaction to give 83% yield (Table 1, entry 12) of the product. Shorter or longer reaction time than 24 h and lower or higher temperature than 120 °C decelerated the reaction rate and led to lower yields (Table 1, entries 1–11). The reaction is very slow in water; use of DMAc–water (1 : 1) mixture results in 3% yield indicating that this coupling process is fairly sensitive to water (Table 1, entry 7). In the absence of base, reaction fails completely (Table 1, entry 5). Among the several solvents tested, DMF, CH₃CN and DMSO were less effective compared to DMAc (Table 1, entries 1–4). Bases such as Cs₂CO₃, K₃PO₄, K₂CO₃, KOH and K^t-OBu are found to facilitate the coupling reaction. Among them K₂CO₃ is the better base which gave good yield when compared to other bases (Table 1, entries 6–10). The *N*-arylation of imidazole is also found to be highly sensitive to reaction temperature and time. At lower temperature (30–90 °C) or lower reaction time (6–12 h), the reaction proceeds slowly or moderately (Table 1, entries 1–11). These preliminary results revealed that Fe–CuO is a good catalyst for *N*-arylation of imidazole in the presence of K₂CO₃ in DMAc solvent at 120 °C, which afforded the corresponding *N*-arylated product in 83% yield after 24 h (Table 1, entry 12). Once the conditions were found, other aryl halides were subjected to the same reaction under identical conditions and the results are

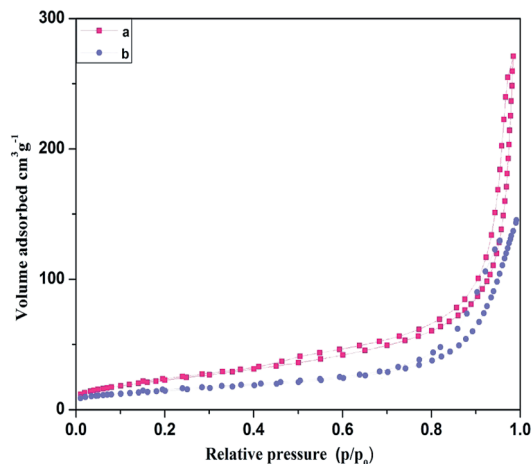
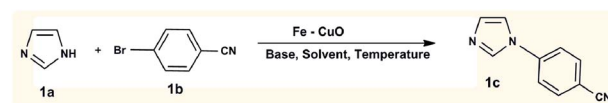


Fig. 5 N₂ adsorption–desorption isotherm of (a) as prepared and (b) calcined Fe–CuO nanocatalyst.

Table 1 Optimization of the reaction conditions for the Fe–CuO-catalyzed *N*-arylation of imidazole (1a) with 4-bromobenzonitrile (1b) to obtain *N*-arylated imidazole (1c)^a



Entry	Solvent	Base	Time (h)	Temperature (°C)	Yield ^b (%)
1	DMF	K ₂ CO ₃	10	70	16
2	DMSO	K ₂ CO ₃	8	80	18
3	DMAc	K ₂ CO ₃	30	140	53
4	CH ₃ CN	KOH	12	110	3
5	DMAc	—	24	110	NR
6	DMAc	CS ₂ CO ₃	20	40	7
7	DMAc–H ₂ O	NaOH	6	50	3
8	DMAc	K ^t -OBu	10	80	9
9	DMAc	K ₃ PO ₄	15	75	5
10	DMAc	K ₃ PO ₄	22	60	6
11	DMAc	K ₂ CO ₃	24	120	83
12	DMAc	K ₂ CO ₃	16	100	71
13	DMAc	K ₂ CO ₃	40	110	77

^a All the reactions were performed with Fe–CuO (10 mg), 1 mmol (182 mg) of 4-bromobenzonitrile, 1.2 mmol (81 mg) of imidazole, and 2.0 mmol of base in 4 mL of solvent at 120 °C for 24 h. ^b GC yield, NR = no reaction.

presented in Table 2. Bromo is the better leaving group compared to chloro and fluoro groups (the leaving group ability of halogens is in the order of I > Br > Cl > F). Hence, the aryl bromides react faster compared to the aryl chlorides and fluorides (Table 2, entries 3, 10 and 11). It is noteworthy to mention that C–N cross-coupling reactions with aryl chlorides rarely gave good yields. Even then, the aryl chlorides are also coupled with imidazole to afford the corresponding *N*-arylated products in excellent yields (Table 2, entries 7–10) which was not so in some other catalytic systems.^{43,44} The *para*-substituted aryl halides

Table 2 Fe–CuO-catalyzed *N*-arylation of imidazole with various aryl halides^a

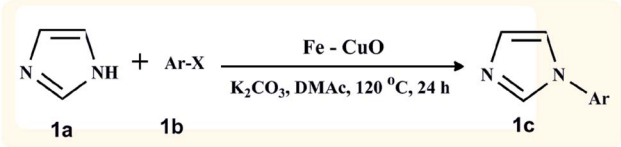
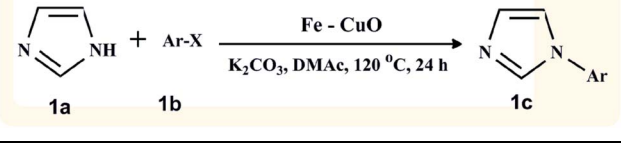
			
Entry	Aryl halides (1b)	Product (1c)	GC yield (%)
1			90 (68) ^b
2			83 (77) ^b
3			92 (84) ^b
4			62 (59) ^b
5			83 (82) ^b
6			89 (83) ^b
7			94 (90) ^b
8			82 (78) ^b
9			76 (57) ^b
10			99 (89) ^b
11			74 (70) ^b

Table 2 (Contd.)

			
Entry	Aryl halides (1b)	Product (1c)	GC yield (%)
12			99 (94) ^b
13 ^c			5 (3) ^b

^a All the reactions were performed with Fe–CuO (10 mg), 1 mmol (182 mg) of 4-bromobenzonitrile, 1.2 mmol (81 mg) of imidazole and 2.0 mmol of K₂CO₃ in 4 mL of solvent at 120 °C for 24 h. ^b Isolated yield.

^c Reaction performed with bare γ-FeOOH.

provided a better yield in comparison to the *ortho*-substituted (Table 2, entries 4 and 11) aryl halides. The low yield of *ortho*-substituted aryl halides may be due to the steric effect.²⁵ Gopiraman *et al.*, used CNTs supported CuO NPs as a catalyst for the *N*-arylation with the similar substrates under similar reaction conditions. But in many cases the present catalytic system showed higher activity. For instance the reaction of 4-chlorobenzoic acid with imidazole gave excellent yield (99%) of *N*-arylated product in the present catalytic system (Table 2, entry 10) whereas the same product was obtained only in 88% yield by Gopiraman *et al.*²⁶ Punniyamurthy and co-workers⁴⁵ exploited the high surface area and reactive morphology of the CuO nanoparticles for successful C–N cross-coupling reactions. Although the results are promising for the *N*-arylation reaction, only low yields were obtained when aryl chlorides were used. Park and co-workers⁴⁶ used acetylene-carbon-immobilized CuO hollow nano spheres for *N*-arylation reactions at higher temperature (*i.e.* 180 °C) to get good yield and temperature lower than 180 °C led to lower yields but the present catalytic system provided excellent yields at 120 °C. Usually C–F bond activation is not so easy; but the aryl fluorides are also coupled with imidazole to afford the corresponding *N*-arylated products in excellent yields (Table 2, entries 11 and 12). Especially, 4-fluoroacetophenone gave an excellent yield of 99% (Table 2, entry 12). Karvembu and co-workers reported that the CuO nanoparticles catalyzed C–N cross coupling of benzimidazole with 4-fluoroacetophenone to form *N*-arylated benzimidazole product under identical reaction conditions but the yield was low (67%)²⁵ as compared with the present catalytic system (99%) (entry 11). Suramwar *et al.*,⁴⁷ have reported the ligand-free

copper oxide nanocatalyst for *N*-arylation of triazole with various aryl halides. They found that the copper oxide catalyst showed very high conversions when the reaction was carried out in DMF or toluene as the solvent and difficulty in separation of product limits the method. No significant yield was observed with γ -FeOOH (Table 2, entry 13). Nevertheless the activity enhanced predominantly by the loading of CuO (Table 2, entries 1–12). Bimetallic systems generally showed better activity than monometallic systems,^{45–48} which was evident in the present protocol as well. Niranjana *et al.*, reported that the bimetallic system possesses a much higher surface area and hence much higher activity than those monometallic systems.⁴⁹ A similar result was observed previously,⁵⁰ in which Fe–Cu bimetallic system showed better catalytic performance than pure Fe₂O₃. Hence, many researchers are involved in the development of bimetallic nanocomposite system for a targeted reaction.^{51–54} Notably, the Fe–CuO catalyst yielded the *N*-arylated imidazole product smoothly, which is promising and predominant over the previous reports.⁵⁰ To expand the scope of this protocol further, other nitrogen containing heterocycles such as benzimidazole, carbazole, pyrrole, indole, and triazole are coupled with 4-bromobenzonitrile to give the corresponding *N*-arylated products in good yield (Table 3). In order to show that Fe–CuO nanoparticles are heterogeneous catalysts, a hot filtration test was performed for *N*-arylation of imidazole with 4-bromobenzonitrile. In a typical experiment, the catalyst was separated out from the reaction mixture after 12 h by using a magnet, and then stirring was continued without the catalyst. The reaction was allowed to proceed further for 12 h and the yield was determined by GC at each 4 h intervals. The result indicated that no further conversion occurred after the nanocatalyst was separated out from the reaction mixture, which indicates that the *N*-arylation reaction of imidazole occurred only due to solid Fe–CuO (see ESI – S6†). Isolation and reuse of the catalyst are the crucial requirements for any practical application in terms of cost and environmental protection. It is well known that magnetic separation makes the recovery of catalysts from the reaction medium much easier than the traditional separation procedures such as filtration and centrifugation. In the present system, the catalyst can be easily recovered by using an external magnet as shown in Fig. 1. Once the reaction was completed, the catalyst was trapped with the help of a magnet, washed with ethyl acetate, air dried and used directly in the next cycle. The catalyst could be reused six times without any significant detrimental effect on the yield (see ESI – S7†).

Surface area and particle size play a vital role in heterogeneous catalysis. Owing to the highly active surface area of MNPs, they are usually employed as a heterogeneous nanocatalyst in various reactions and facilitate better yields. Particularly, MNPs having the size of fewer than 10 nm exhibited a dramatic catalytic activity.⁵⁵ Therefore, the effect of Fe–CuO particle size on catalytic efficiency in terms of yields has been investigated. For this purpose, another nanocatalyst with Fe–CuO size of around 33 nm was prepared following the same procedure, but the calcination was carried out at 500 °C for 3 h. It is well known that MNPs can easily agglomerate to form bigger particles particularly at higher temperature due to their high specific

Table 3 Fe–CuO-catalyzed *N*-arylation of various heterocycles with 4-bromobenzonitrile^a

Entry	Het-NH	Product	Time (h)	Yield ^b (%)
1			20	72
2			24	83
3			24	98
4			16	65
5			24	67

^a All the reactions were performed with Fe–CuO (10 mg), 1 mmol (182 mg) of 4-bromobenzonitrile, 1.2 mmol of heterocycles and 2.0 mmol of K₂CO₃ in 4 mL of solvent at 120 °C. ^b GC yield.

surface energy.⁵⁶ Here, it is postulated that the Fe–CuO might be agglomerated to form bigger Fe–CuO (33 nm) at the calcination temperature of 500 °C. The increases in the temperature from 30 to 500 °C increased the size of Fe–CuO from 7 nm to 33 nm; this suggests that the size of Fe–CuO depends on the temperature. The Fe–CuO catalyst (33 nm) has a BET surface area of 50.31 m² g^{−1} with a pore volume of 0.224 cm³ g^{−1} (Fig. 5).

The surface area per unit mass (*S*) of 7 nm sized Fe–CuO was found to be 83.1989 m² g^{−1} with a pore volume of 0.419 cm³ g^{−1}. Both the nanocatalysts were employed in the *N*-arylation reaction of imidazole with various aryl halides (Table 3). As expected, 7 nm Fe–CuO exhibited a good catalytic activity in comparison to the one which has 33 nm size (Table 4). When the size of Fe–CuO decreases, the surface area per unit mass (*S*) certainly increases. Consequently, a larger number of active sites are available.⁵⁷ Thus, Fe–CuO having the particle size of 7 nm showed excellent catalytic activity.

A plausible three-step mechanism for the Fe–CuO-catalyzed *N*-arylation is proposed. The catalytic reaction is expected to take place *via* adsorption followed by desorption. In the first step, the aryl halide adsorbed over the surface of Fe–CuO nanocomposites to form intermediate-II. At the same time base

Table 4 Catalytic activity of Fe–CuO (33 nm) and Fe–CuO (7 nm) toward *N*-arylation of imidazole with various aryl halides^a

$\text{Imidazole (1a)} + \text{Ar-X (1b)} \xrightarrow[\text{K}_2\text{CO}_3, \text{DMAc, 120 } ^\circ\text{C, 24 h}]{\text{Fe-CuO}} \text{N-arylated imidazole (1c)}$				
Entry	Ar-X (1b)	Product (1c)	Yield ^b (%)	Yield ^c (%)
1			90	43
2			92	56
3			94	28
4			99	47

^a All the reactions were performed with Fe–CuO (10 mg), 1 mmol (182 mg) of 4-bromobenzonitrile, 1.2 mmol (81 mg) of imidazole and 2.0 mmol of K₂CO₃ in 4 mL of DMAc at 120 °C for 24 h. ^b GC yield of the product when the particle size of Fe–CuO is 7 nm. ^c GC yield of the product when the particle size of Fe–CuO is 33 nm.

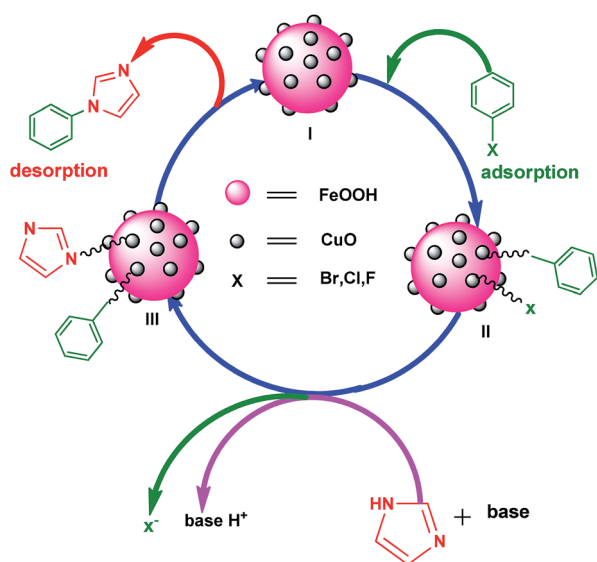


Fig. 6 Proposed mechanism for Fe–CuO-catalyzed *N*-arylation of imidazole with aryl halides.

removed proton from the imidazole which further displaced the halide ion from the surface of the catalyst. The imidazole anion attacks the phenyl cation to form *N*-arylated imidazole. In the final step the desired *N*-arylated imidazole product desorbed from the surface of the catalyst to complete the catalytic cycle (Fig. 6).

Conclusions

In summary a simple, highly efficient, economical, environmental friendly, easily separable and reusable heterogeneous Fe–CuO magnetic catalyst was prepared by a very simple precipitation technique. It showed a good catalytic activity towards the *N*-arylation of imidazole with various aryl halides. More significantly, this catalyst could be easily recovered by magnetic separation and reused for several cycles without significant loss of activity. This catalyst solves the basic problems of catalyst separation and recovery and thus this protocol may find widespread use for the preparation of *N*-arylated heterocycles.

Experimental section

The reagents used in the synthesis, such as FeSO₄·7H₂O and CuSO₄ were purchased from Sigma-Aldrich and used as received without any further purification. ¹H NMR spectra were recorded at 250 and 400 MHz, and ¹³C NMR spectra were recorded at 62.9 and 100 MHz in CDCl₃ using TMS as an internal standard. Column chromatography was carried out on silica gel 60 Merck (230–240 mesh) in glass columns (2 or 3 cm diameter) using 15–30 grams of silica gel per one gram of the crude mixture. The morphology of the catalyst was investigated on scanning electron microscope (Hitachi COM-S-4200 SEM) and transmission electron microscope (Jeol, JEM-2100F TEM) with accelerating voltage of 120 kV. XRD analyses were performed on a Bruker D-8 Advance diffractometer using Cu Kα radiation (λ = 1.5418 Å). The Fourier transform infrared (FT-IR) spectra were recorded (Jasco 460 Plus FT-IR) as KBr pellets in the wavenumber range 4000–400 cm^{−1}. The oxidation state of the metals was determined by X-ray photoelectron spectroscopy (Kratos Axis-Ultra DLD, Kratos Analytical Ltd, Japan). The magnetic measurements were carried out on a vibrating sample magnetometer (Lakeshore, Model-7400) with an applied field between −15 000 and 15 000 (Oe) at room temperature. The Cu loading was determined by inductively coupled plasma optical emission spectrometry (ICP-OES, Élan DRC-e, and Perkin Elmer). Thermo gravimetric analysis was made with (SII EXSTAR 6200) TG/DTA analyzer. Raman spectrometer (Hololab 5000, Kaiser Optical Systems Inc.) was applied to examine the interaction between copper oxide nanoparticles (CuONPs) and lepidocrocite. The argon laser was operated at 532 nm with a Kaiser holographic edge. The specific surface area of the magnetic catalyst was determined by BET analysis while pore volume was determined by the Barrett–Joyner–Halenda (BJH) method using Quanta Chrome (NOVAe) surface area analyzer.

Preparation of lepidocrocite

The lepidocrocite and Fe–CuO were prepared following the literature.²⁸ To prepare lepidocrocite, $\text{FeSO}_4 \cdot 7\text{H}_2\text{O}$ (0.13 M) was dissolved in distilled water (100 mL). Then NH_4OH (10%) was added drop wise into the suspension until the pH of the solution was adjusted to 6.5. The mixture was stirred vigorously for 4 h. The black precipitate was collected from the solution by an external magnet and washed with double distilled water. Finally the black product was dried under vacuum at 80 °C.

Preparation of Fe–CuO catalyst

$\text{CuSO}_4 \cdot 5\text{H}_2\text{O}$ (0.005 M), was dissolved in distilled water (50 mL). $\gamma\text{-FeOOH}$ (0.51 g) was then dispersed in the above solution and sonicated to obtain a uniform suspension. The suspension was vigorously stirred at room temperature for 50 min to ensure that enough Cu^{2+} had been adsorbed on the surface of $\gamma\text{-FeOOH}$. Then the pH was adjusted to 6.5 by adding 10% NH_4OH . The mixture was stirred vigorously for 4 h. The precipitated black product was collected from the solution using an external magnet (Fig. 1), washed with water, and dried under vacuum at 80 °C.

Procedure for N-arylation of imidazole

In a typical procedure, Fe–CuO catalyst (10 mg) was added into a mixture of imidazole (1.2 mmol, 81 mg), 4-bromobenzonitrile (1 mmol, 182 mg) and K_2CO_3 (2 mmol, 276 mg) in DMAc (4 mL), stirred under air atmosphere at 120 °C for 24 h. After the complete consumption of starting materials as monitored by thin layer chromatography (TLC), the catalyst was separated by magnetic decantation and washed well with diethyl ether and dried in an oven at 110 °C for 3 h. The organic layer was partitioned between 10 mL of ethyl acetate and 5 mL of saturated aqueous NaCl solution. The product was extracted with ethyl acetate and dried over anhydrous sodium sulfate. The yield of product was determined by GC. Finally, the organic layer was concentrated to obtain N-arylated imidazole.

Product analysis

In order to confirm the formation of the product, samples of both reactants and products were dissolved in ethyl acetate and analyzed by gas chromatograph (Shimadzu 2010) equipped with 5% diphenyl and 95% dimethyl polysiloxane, Restek-5 capillary column (0.32 mm dia, 60 m length and 0.32 mm dia) and a flame ionization detector (FID). The initial column temperature was increased from 60 to 150 °C at the rate of 10 °C min^{-1} and then to 220 °C at the rate of 40 °C min^{-1} . N_2 was used as a carrier gas. During the product analysis the temperatures of the FID and injection port were kept constant at 150 and 250 °C respectively.

Acknowledgements

One of the authors R.S. is thankful to the Department of Science and Technology, Government of India, New Delhi for the award of research fellowship under the DST PURSE programme.

Notes and references

- 1 F. Diederich and A. de Meijere, *Metal-Catalyzed Cross-Coupling Reactions*, Wiley-VCH, Weinheim, 2004.
- 2 J. P. Wolfe, S. Wagaw, J. F. Marcoux and S. L. Buchwald, *Acc. Chem. Res.*, 1998, **31**, 805.
- 3 G. R. Martinez, K. A. M. Walker, D. R. Hirschfield, J. J. Bruno, D. S. Yang and P. J. Maloney, *J. Med. Chem.*, 1992, **35**, 620.
- 4 J. Ohmori, M. S. Sasamata, M. Okada and S. Sakamoto, *J. Med. Chem.*, 1996, **39**, 3971.
- 5 I. Sircar, R. E. Weishaar, D. Kobylarz, H. Moos and J. A. Bristol, *J. Med. Chem.*, 1987, **30**, 1955.
- 6 P. Cozzi, G. Carganico, D. Fusar, M. Grossoni, M. Menichincheri, V. Pinciroli, R. Tonani, F. Vaghi and P. Salvati, *J. Med. Chem.*, 1993, **36**, 2964.
- 7 Y. S. Lo, J. C. Nolan, T. H. Maren, W. J. Welstead Jr, D. F. Gripshover and D. A. Shamblee, *J. Med. Chem.*, 1992, **35**, 4790.
- 8 D. Maiti, B. P. Fors, J. L. Henderson, Y. Nakamura and S. L. Buchwald, *Chem. Sci.*, 2011, **2**, 57.
- 9 W. Yi, W. Zhiqing, W. Lixia, L. Zhengkai and Z. Xiangge, *Chem.-Eur. J.*, 2009, **15**, 8971.
- 10 S. G. Babu and R. Karvembu, *Ind. Eng. Chem. Res.*, 2011, **50**, 9594.
- 11 M. L. Kantam, Y. Jagjit, L. Soumi, S. Bojja and J. Shailendra, *Adv. Synth. Catal.*, 2007, **349**, 1938.
- 12 S. Mandal, D. Roy, R. V. Chaudhari and M. Sastry, *Chem. Mater.*, 2004, **16**, 3714.
- 13 P. Poisson, J. P. Brunelle and P. Nortier, *Catalyst Supports and Supported Catalysts*, ed. A. B. Stiles, Wiley VCH, Butterworth, Boston, 1987, pp. 11–55.
- 14 S. Shylesh, V. Schunemann and W. R. Thiel, *Angew. Chem., Int. Ed.*, 2010, **49**, 3428.
- 15 J. Fan and Y. Gao, *J. Exp. Nanosci.*, 2006, **1**, 457.
- 16 Y. Zhu, J. Shen, K. Zhou, C. Chen, X. Yang and C. Li, *J. Phys. Chem. C*, 2011, **115**, 1614.
- 17 S. R. Kale, S. S. Kahandal, M. B. Gawande and R. V. Jayaram, *RSC Adv.*, 2013, **3**, 8184.
- 18 M. B. Gawande, P. S. Branco and R. S. Varma, *Chem. Soc. Rev.*, 2013, **42**, 3371.
- 19 R. B. N. Baig and R. S. Varma, *Chem. Commun.*, 2012, **48**, 2582.
- 20 P. H. Li, B. L. Li, Z. M. An, L. P. Mo, Z. S. Cui and Z. H. Zhang, *Adv. Synth. Catal.*, 2013, **355**, 2952.
- 21 M. J. Aliaga, D. J. Ramon and M. Yus, *Org. Biomol. Chem.*, 2010, **8**, 43.
- 22 M. Liu, X. G. Peng, W. Sun, Y. W. Zhao and C. G. Xia, *Org. Lett.*, 2008, **10**, 3933.
- 23 S. G. Babu, P. A. Priyadarsini and R. Karvembu, *Appl. Catal., A*, 2011, **392**, 218.
- 24 S. G. Babu and R. Karvembu, *Tetrahedron Lett.*, 2013, **54**, 1677.
- 25 S. G. Babu, N. Neelakandeswari, N. Dharmaraj, S. David Jackson and R. Karvembu, *RSC Adv.*, 2013, **3**, 7774.
- 26 M. Gopiraman, S. G. Babu, Z. Khatri, W. Kai, Y. A. Kim, M. Endo, R. Karvembu and I. S. Kim, *Carbon*, 2013, **62**, 135.

- 27 D. Takagi, Y. Homma, H. Hibino, S. Suzuki and Y. Kobayashi, *Nano Lett.*, 2006, **6**, 2642.
- 28 K. Inouye, K. Ichimura, K. Kaneko and T. Ishikawa, *Corros. Sci.*, 1976, **16**, 507.
- 29 R. M. Cornell and U. Schwertmann, *The Iron Oxides*, VCH, New York, 2nd edn, 2003.
- 30 M. Ristic, S. Music and M. Godec, *J. Alloys Compd.*, 2006, **417**, 292.
- 31 G. Socrates, *Infrared and Raman Characteristic Frequencies*, John Wiley & Sons Ltd, New York, 3rd edn, 2001.
- 32 D. Liu, S. Yang and S. T. Lee, *J. Phys. Chem. C*, 2008, **112**, 7110.
- 33 S. Rahman, K. Nadeem, M. A. Rehman, M. Mumtaz, S. Naeem and I. L. Papst, *Ceram. Int.*, 2013, **39**, 5235.
- 34 T. Yamashita and P. Hayes, *Appl. Surf. Sci.*, 2008, **254**, 2441.
- 35 J. Ghijsen, L. H. Tjeng, J. Van, H. Eskes, J. Westerink, G. A. Sawatzky and M. T. Czyzyk, *Phys. Rev. B: Condens. Matter Mater. Phys.*, 1988, **38**, 11322.
- 36 N. S. McIntyre and M. G. Cook, *Anal. Chem.*, 1975, **47**, 2208.
- 37 M. Hanesch, *Geophys. J. Int.*, 2009, **177**, 941.
- 38 J. F. Xu, W. Ji, Z. X. Shen, W. S. Li, S. H. Tang, X. R. Ye, D. Z. Jia and X. Q. Xin, *J. Raman Spectrosc.*, 1999, **30**, 413.
- 39 A. V. Shchukarev and D. V. Korolkov, *Cent. Eur. J. Chem.*, 2004, **2**, 347.
- 40 D. L. A. de Faria, S. V. Silva and M. T. de Oliveira, *J. Raman Spectrosc.*, 1997, **28**, 873.
- 41 Y. Zhu, K. Mimura and M. Isshiki, *Mater. Trans.*, 2002, **4**, 2173.
- 42 K. Inouye, K. Ichimura, K. Kaneko and T. Ishikawa, *Corros. Sci.*, 1976, **16**, 507.
- 43 H. J. Cristau, P. P. Cellier, J. F. Spindler and M. Taillefer, *Eur. J. Org. Chem.*, 2004, **256**, 695.
- 44 M. Taillefer, N. Xia and A. Ouali, *Angew. Chem., Int. Ed.*, 2007, **46**, 934.
- 45 L. Rout, S. Jammi and T. Punniyamurthy, *Org. Lett.*, 2009, **74**, 3397.
- 46 A. Y. Kim, H. J. Lee, J. C. Park, H. Kang, H. Yang, H. Song and K. H. Park, *Molecule*, 2009, **14**, 5169.
- 47 N. V. Suramwar, S. R. Thakare and N. T. Khaty, *J. Mol. Catal. A: Chem.*, 2012, **359**, 28.
- 48 J. A. Rodriguez, *Surf. Sci. Rep.*, 1996, **24**, 223.
- 49 P. Niranjana, J. A. Kumar, M. Sasmita and R. S. M. Ranjan, *Tetrahedron Lett.*, 2011, **52**, 1924.
- 50 W. M. Shaheen, *Mater. Sci. Eng., A*, 2007, **445**, 113.
- 51 I. E. Wachs, *Catal. Today*, 2005, **100**, 79.
- 52 M. Taillefer, N. Xia and A. Ouali, *Angew. Chem., Int. Ed.*, 2007, **46**, 934.
- 53 Z. Wang, H. Fu, Y. Jiang and Y. Zhao, *Synlett*, 2008, 2540.
- 54 D. Guo, H. Huang, Y. Zhou, J. Xu, H. Jiang, K. Chen and H. Liu, *Green Chem.*, 2010, **12**, 276.
- 55 G. A. E. Shobaky and N. M. Deraz, *Mater. Lett.*, 2001, **47**, 231.
- 56 S. H. Joo, J. Y. Park, J. R. Renzas, D. R. Butcher, W. Huang and G. Somorjai, *Nano Lett.*, 2010, **10**, 2709.
- 57 A. T. Bell, *Science*, 2003, **299**, 1688.